Electronic structure of the Pb/Si(111)-($\sqrt{7}\times\sqrt{3}$) surface reconstruction: A first-principles study

Chia-Hsiu Hsu,[1] Feng-Chuan Chuang,[1,*] Marvin A. Albao,[2] and V. Yeh[3]

[1]*Department of Physics, National Sun Yat-Sen University, Kaohsiung 804, Taiwan*
[2]*Institute of Mathematical Sciences and Physics, University of the Philippines Los Baños, College, Laguna 4031, Philippines*
[3]*Department of Physics, National Dong Hwa University, Hualien 97401, Taiwan*

Electronic structures of the Pb/Si(111)-($\sqrt{7}\times\sqrt{3}$) surface reconstruction were reexamined using first-principles calculations. The band structures of the proposed models were analyzed in detail. Our results show that the calculated bands for the H3 model at lead coverage of 1.2 ML are in good agreement with the identified bands in the angle-resolved photoemission study [Phys. Rev. B **75**, 075329 (2007)]. Lastly, the work functions of the $\sqrt{7}\times\sqrt{3}$ and $\sqrt{3}\times\sqrt{3}$ phases were also calculated and compared with experimental measurements.

PACS number(s): 73.20.At, 68.35.B−, 68.43.Bc

In recent years, metal overlayers grown on a semiconductor surface have generated huge research interests in recent years owing to their low dimensional electronic properties. Two of the most intriguing characteristics in prototypical Pb/Si(111) system, the QSE-driven (quantum size effects) growth mode[1–3] and the Devil's staircase,[4,5] have been studied extensively over the past decade. It was suggested that the work function of the substrate affects the outcome of QSE-driven growth.[1] In the Devil's staircase one observes the presence of as many phases as possible at a small Pb coverage interval between 1.2 and 1.3 ML. These phases are constructed from a linear combination of $\sqrt{7}\times\sqrt{3}$(hereafter $\sqrt{7}$) and $\sqrt{3}\times\sqrt{3}$ (hereafter $\sqrt{3}$) unit cells.[4,5] These intriguing characteristics suggest a need for a detailed investigation on the electronic structures of the $\sqrt{7}$ and $\sqrt{3}$ phase in order to better understand the system.

Numerous studies on the $\sqrt{7}$ phase have been performed and several structural models at two different Pb coverages have been proposed. The model by Hwang *et al.*[6–8] contains five Pb atoms per supercell corresponding to 1.0 ML. Three Pb atoms form a trimer centered at the H3 site, while the other two Pb atoms are at T1 sites. By contrast, the model proposed by Kumpf *et al.*[9] contains six Pb atoms corresponding to 1.2 ML. Four of these Pb atoms are essentially at the T1 sites, while another is located on a bridge position above two Si atoms. Finally, the sixth Pb atom is located at a H3 site.

The experimentally proposed models were then examined by Brochard *et al.* using first-principles calculations.[10] Their results showed that the actual Pb coverage of the $\sqrt{7}$ phase should correspond to 1.2 ML.[9] A related theoretical study by Chan *et al.*[11] further identified two energetically degenerate models with similar atomic structures at 1.2 ML. The first, so-called H3 model, turns out to be the Kumpf model[9] and agrees with the experimental STM results better than the T4 model. The latter is obtained by removing the Pb atom in the H3 model and placing it instead at the T4 site.

Another interesting phenomenon observed in metal overlayers on the semiconductor surface is that the surfaces exhibit either two-dimensional (2D) (Refs. 12 and 13) or one-dimensional (1D) metallic character.[14] The dense Pb layers on Si(111) seem to belong to 2D metallic systems based on the recent angle-resolved and high-resolution core-level pho-toemission studies by Choi *et al.*[15,16] Very recently, motivated to understand better the quantum size effect, the work function difference between the $\sqrt{3}$ and $\sqrt{7}$ phases was measured by observing the Gunlach oscillation.[17–19] In view of these two additional experimental data for the $\sqrt{7}$ phase, it is highly desirable to revisit its electronic properties in greater details.

In this Brief Report, we re-examined the atomic and electronic structures of the Pb/Si(111)-$\sqrt{7}$ surface using first-principles calculations and focused on their band structures and work functions. Our results show that the calculated bands of the H3 model at 1.2 ML are in agreement with the experimental ARPES data, suggesting that the experiment[15] was performed at this Pb coverage.

The calculations were carried out within the generalized gradient approximation[20] to density functional theory[21] using projector-augmented-wave potentials.[22,23] The kinetic energy cutoff was set to 245.3 eV (18.03 Ry) and the 7×7 and 5×7 Monkhorst-Pack grids were used to sample the surface Brillouin zones (SBZ) for the $\sqrt{3}$ and $\sqrt{7}$ phases, respectively. The relaxation method and the thickness of the substrate are the same as that employed in our previous studies.[24]

The relative surface energy, ΔE_s, with respect to the lowest energy model of the $\sqrt{7}$ phase at 1.2 ML is calculated according to the relation

$$\Delta E_s = \frac{E_{model}}{A} - \frac{E_{H3-\sqrt{7}}}{5} - (\theta_{Pb} - 1.2) \times \mu_{Pb}. \qquad (1)$$

In the above, $E_{H3-\sqrt{7}}$ and E_{model} are the total energies of the $\sqrt{7}$ phase and other proposed models, respectively. Also, the surface area, A, of the reconstruction has the value $A=3$ for the $\sqrt{3}$ phase and $A=5$ for the $\sqrt{7}$ phase. μ_{Pb}, on the other hand, represents the chemical potential of Pb, while θ_{Pb} is the Pb coverage of the proposed model.

The structural models for $\sqrt{7}$ are illustrated in Fig. 1. The relative surface energies of the known models, listed in Table I, are obtained by setting the bulk energy of Pb to the chemical potential. Our results indicate that the originally proposed trimer model is unstable. However, we identified a new model T1′ in which two of the Pb atoms at T1 sites are slightly distorted, while the rest three Pb atoms remain at T1 sites. The T1′ model shown in Fig. 1(c) for $\theta_{Pb}=1.0$ ML is
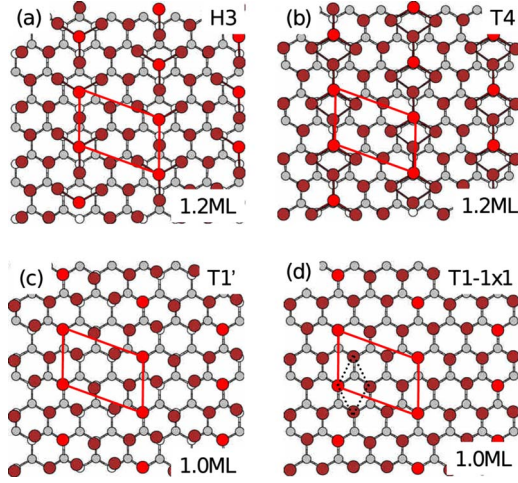
FIG. 1. (Color online) The optimized atomic structures of the (a) H3, (b) T4, and (c) T1′ models for the $\sqrt{7}$ phase. (d) shows the T1 model for the 1×1 phase, with the 1×1 unit cell outlined with dotted lines. White circles and gray spheres indicate the silicon atoms of the first and second layers, respectively, while dark (red and dark red) spheres represent the Pb atoms. The $\sqrt{7} \times \sqrt{3}$ supercell is outlined with the gray (red) solid lines.

not as stable as the H3 [Fig. 1(a)] and T4 [Fig. 1(b)] models for $\theta_{Pb} = 1.2$ ML. However, the T1′$-\sqrt{7}$ model has a lower total energy than the T1-1×1 phase [Fig. 1(d)] by 3 meV per 1×1 cell, where in the latter the Pb atoms all reside on the T1 sites. This energy difference is too small and could not be used to explain the phase transition from 1×1 to $\sqrt{7}$ at low temperature. Next, we further verified the stability due to the chemical potential of the Pb atom. Our results on the relative stabilities of models so far are in agreement with the studies by Brochard *et al.* and Chan *et al.*[10,11]

The band structures of four models (e.g., H3-$\sqrt{7}$ and T4-$\sqrt{7}$ models for $\theta_{Pb} = 1.2$ ML, as well as the T1′-$\sqrt{7}$ and T1-1×1 models for $\theta_{Pb} = 1.0$ ML) were presented and compared with experimental data. The surface Brillouin zones for the $\sqrt{7}$ and 1×1 phases are illustrated in Fig. 2. Certain special points are indicated and the choice of the band dispersion directions $[11\bar{2}]$ and $[\bar{1}10]$ is the same with that used

TABLE I. The relative surface energies, ΔE_s (meV per 1×1 cell), with respect to H3$-\sqrt{7}$ model and work functions, ϕ (eV), of numerous models.

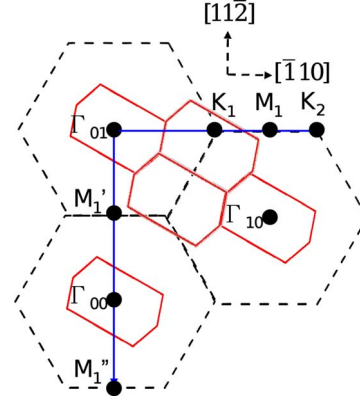| Label	Supercell	θ_{Pb}	ΔE_s	ϕ
H3$-\sqrt{7}$	$\sqrt{7} \times \sqrt{3}$	1.2	0	4.15
T4$-\sqrt{7}$	$\sqrt{7} \times \sqrt{3}$	1.2	3	4.13
T1′$-\sqrt{7}$	$\sqrt{7} \times \sqrt{3}$	1.0	95	4.46
T1-1×1	$\sqrt{7} \times \sqrt{3}$	1.0	98	4.62
T4$-\sqrt{3}$-dense	$\sqrt{3} \times \sqrt{3}$	4/3	11	3.86
H3$-\sqrt{3}$-dense	$\sqrt{3} \times \sqrt{3}$	4/3	17	3.85
T4$-\sqrt{3}$	$\sqrt{3} \times \sqrt{3}$	1/3	199	3.85
H3$-\sqrt{3}$	$\sqrt{3} \times \sqrt{3}$	1/3	309	3.83
7×7	7×7	0	408	4.33

FIG. 2. (Color online) Surface Brillouin zones for the Pb/Si(111)-($\sqrt{7}$) surface reconstruction. Certain special points are indicated. The dashed lines are used to delineate the 1×1 SBZ. The solid (red) lines are the $\sqrt{7} \times \sqrt{3}$ SBZ.

in the experiment.[15] The diameter of the circles in the plot is proportional to the contribution from the surface Pb atoms. The dashed lines (S1, S2, S3, S1′, S4, S5, and S6) in Figs. 3 and 4 are reproduced from the identified bands in the ARPES experiment.[15]

The energy difference between the H3 and T4 models for $\sqrt{7}$ is rather small (3 meV per 1×1 cell). The atomic structures of H3 and T4 models are almost identical except for the two particular atomic positions. Thus, the T4 model can be obtained from the H3 model by selectively shifting the Pb atom at H3 toward the T4 site by 0.8 Å. This distortion is less than the typical Pb-Pb bond distance and thus does not result in any significant change in the rest of the geometry. Furthermore, the calculated surface bands contributed from the Pb overlayer for H3 and T4 models are indistinguishable, seemingly suggesting very weak interaction between the Pb overlayer and the Si substrate. The same phenomena was also observed in the $\sqrt{3}$-dense phase. The dense T4-$\sqrt{3}$ and H3-$\sqrt{3}$ differ in energy by 6 meV per 1×1 cell. The Pb layers of the two models are in fact identical and differ in their relative position with respect to the Si substrate. Our additional calculation shows that the surface band structures of the H3 and T4 models for Pb/Ge(111) and Pb/Si(111) $\sqrt{3}$-dense are also indistinguishable, suggesting the same fact that interaction between the Pb layer and Si or Ge substrates are likewise weak. For the $\sqrt{7}$ phase, since the geometries of Pb layers are quite similar, the minor differences between the band structures in the shaded bulk region around the Γ points cannot be used to clearly identify and differentiate between specific Pb configurations.

The following discussion for the H3 model directly applies to the T4 model as well. The band structures of the H3 model along the $\Gamma_{01} - K_1 - M_1 - K_2$ line and along $\Gamma_{01} - M_1'$ $- \Gamma_{00} - M_1''$ line are displayed in Figs. 3(a) and 3(b), respectively, while for the T4 model, the band structures are plotted in Figs. 3(c) and 3(d). In Fig. 3(a), a strong band S1 disperses out of the M_1 point starting at E_f down to -0.9 eV. The calculated band matches the experimental S1 band very well. The ARPES data also reveal two strong and parabolic (green) bands S2 centered on K_1 and K_2, respectively. Our calculated band structure also exhibits this surface band S2.
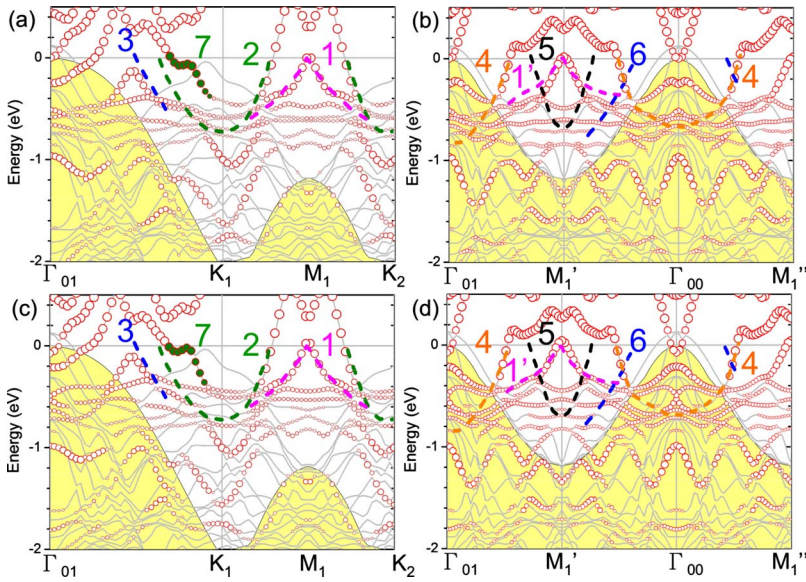
FIG. 3. (Color online) (a) and (b) are band structures of the $\sqrt{7}$-H3 model. (c) and (d) are for the $\sqrt{7}$-T4 model. The projected bulk bands using the same surface cell are shaded. Both Fermi energies of surface band calculation and the projected bulk valence-band maxima are set to zero.

However, the left side of the parabolic S2 band dispersion does not match with the calculated band. Nevertheless, the point (near S3) crossing E_f on left side of parabolic band S2 seems to match the crossing point of the calculated band S7 (indicated by the filled circles). Another metallic band S3 (blue dashed line) identified in the experiment crossing E_f with a very small dispersion compared to that of the S2 (green) band is also partially reproduced in the calculated band. The calculated surface band S3 does not cross E_f, while the experimental band S3 does cross E_f.

In the band map along $\Gamma_{01}-M_1'-\Gamma_{00}-M_1''$ line shown in Fig. 3(b), the band S1$'$ out of M_1 point starting from E_f down to -0.4 eV matches the theoretical band. Moreover, the bands S4 (brown) centered on the Γ_{00} are also reproduced in the calculated band. Another parabolic band S5 around M_1' and M_1'' (the black dashed curves) was identified in the ARPES experiment having its own E_F crossing between those of S1$'$ and S4 bands. However, this S5 band was not seen in the calculated band. Furthermore, the S6 (blue

dashed) band cannot be reproduced in the theoretical band, either. We notice that in the experiment the momentum distribution curves at E_f [Fig. 3(f) of Ref. 15] show a very high photoelectron intensity at Γ_{00} but no surface band was identified below the E_f. Our calculated band structure also demonstrated larger circles at the E_f at Γ_{00} but that the calculated band is below the E_f. In short, the surface bands identified in the experiment were found in the theoretical band structures except for the two bands S5 and S6.

Similarly, the band structure of the T1$'-\sqrt{7}$ model along the $\Gamma_{01}-K_1-M_1-K_2$ and along $\Gamma_{01}-M_1'-\Gamma_{00}-M_1''$ lines are displayed in Figs. 4(a) and 4(b), respectively. In Fig. 4(a), the experimental S1 band strongly dispersing out of the M_1 point does not exactly match with the calculated band. The dispersions of two strong and parabolic bands S2 identified in the ARPES data centered on K_1 and K_2 do not seem to be fully reproduced in our calculated band structure. Likewise, another metallic band S3 crossing E_f with a very small dispersion compared to that of the S2 (green) band could not be
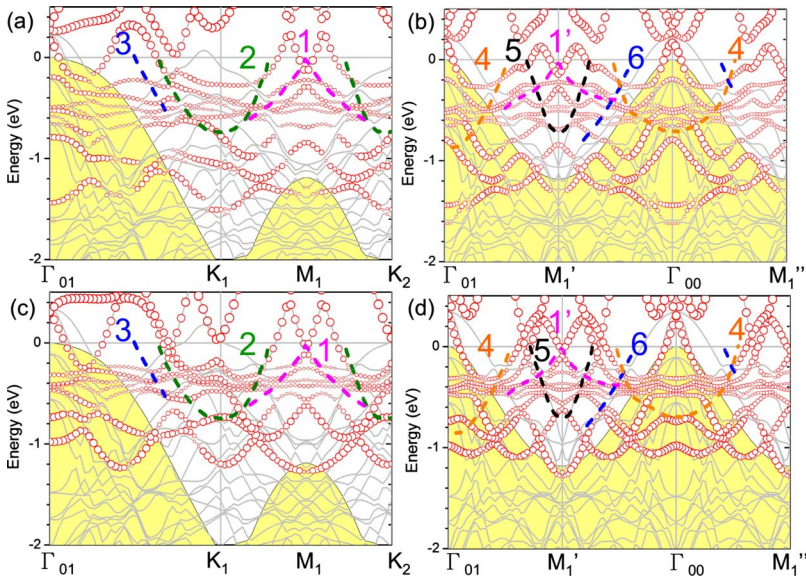

FIG. 4. (Color online) (a) and (b) are band structures of the $\sqrt{7}$-T1$'$ model. (c) and (d) are for the T1-1×1 model calculated using the $\sqrt{7}\times\sqrt{3}$ supercell.

reproduced in the theoretical band, either. It appears that no agreement was found between the calculated bands and the experimental data for this T1′-$\sqrt{7}$ model. In the band map along $\Gamma_{01}-M_1'-\Gamma_{00}-M_1''$ as shown in Fig. 4(b), the agreement appears unsatisfactory. Neither band in the experiment can be seen in the theoretical bands, indicating that the phase in the ARPES experiment was not performed at lead coverage of 1.0 ML.

Our calculated band structures for $\sqrt{7}$ exhibit strong 1×1 features. By analyzing the SBZs in Fig. 2, along the $K_1-M_1-K_2$ direction, the symmetry point of band dispersion at M_1 is expected, while along the $\Gamma_{01}-M_1'-\Gamma_{00}-M_1''$ line, symmetry points at M_1', M_1'', and Γ_{00} are expected. The band dispersions of H3-$\sqrt{7}$ shown in Fig. 3(a) and 3(b) exhibited symmetries at these points (M_1, M_1', M_1'', and Γ_{00}) are confirmed. To highlight the experimental observation that the electronic structure of this phase has a strong 1×1 character with a $\sqrt{7}\times\sqrt{3}$ modulation,[15] the calculated band structures of T1-1×1 using $\sqrt{7}\times\sqrt{3}$ supercells are plotted in Figs. 4(c) and 4(d). By comparing the band structures of T1-1×1 [Figs. 4(c) and 4(d)] and H3-$\sqrt{7}$ [Figs. 3(a) and 3(b)] phases, we are able to theoretically verify the experimental observations. It seems that the surface band dispersions in the H3-$\sqrt{7}$ model were modified relative to those in the T1-1×1 model with the presence of additional Pb atom in the surface. Furthermore, the 2D properties can be observed throughout the band structures mapped along two directions. The S1 and S1′ bands dispersing out of the M_1 points below the E_f show the 2D characters for the holes, while the dispersions above the E_f at Γ points show some similarity for the conduction electrons.

Lastly, the work function was calculated using a double-sided simulation slab with six Si bilayers. The surface reconstructions were manipulated on both sides of the slab. The method of calculating the work function can also be found in the Ref. 25. The work function of various phases were calculated and summarized in Table I. The calculated work function difference between the $\sqrt{3}$-T4 at 1/3 ML and $\sqrt{7}$-H3 phases is around 0.30 eV, while the measured energy shifts in second Gunlach oscillation peaks are around 0.26 eV.[19] By analyzing the energy shifts of Ag/Cu(111) and MgO/Ag(100) surfaces,[18] it was suggested that the second peak is better for work function difference determination when these energy shifts are not constant in low-order oscillation peaks.

In conclusion, electronic structures of the Pb/Si(111)-$\sqrt{7}$ surface reconstruction are reexamined using first-principles calculations. The band structures of numerous models are analyzed in detail. We found that the band structures for the H3 and T4 models at Pb coverage of 1.2 ML have very satisfactory agreement with experimental data. Finally, the calculated work function difference between the $\sqrt{3}$-T4 at 1/3 ML and the $\sqrt{7}$-H3 phases is around 0.30 eV which is in agreement with the experimental measurement.

*Author to whom correspondence should be addressed; fchuang@mail.nsysu.edu.tw

[1] V. Yeh, L. Berbil-Bautista, C. Z. Wang, K. M. Ho, and M. C. Tringides, Phys. Rev. Lett. **85**, 5158 (2000).

[2] S. H. Chang, W. B. Su, W. B. Jian, C. S. Chang, L. J. Chen, and T. T. Tsong, Phys. Rev. B **65**, 245401 (2002).

[3] C. M. Wei and M. Y. Chou, Phys. Rev. B **66**, 233408 (2002).

[4] M. Hupalo, J. Schmalian, and M. C. Tringides, Phys. Rev. Lett. **90**, 216106 (2003).

[5] M. Yakes, V. Yeh, M. Hupalo, and M. C. Tringides, Phys. Rev. B **69**, 224103 (2004).

[6] Ing-Shouh Hwang, R. E. Martinez, Chien Liu, and J. A. Golovchenko, Phys. Rev. B **51**, 10193 (1995).

[7] J. Slezak, P. Mutombo, and V. Chab, Phys. Rev. B **60**, 13328 (1999).

[8] O. Custance, I. Brihuega, J.-Y. Veuillen, J. M. Gomez-Rodriguez, and A. M. Baro, Surf. Sci. **482-485**, 878 (2001).

[9] C. Kumpf, O. Bunk, J. H. Zeysing, M. M. Nielsen, M. Nielsen, R. L. Johnson, and R. Feidenhans'l, Surf. Sci. **448**, L213 (2000).

[10] S. Brochard, Emilio Artacho, O. Custance, I. Brihuega, A. M. Baró, J. M. Soler, and J. M. Gómez-Rodríguez, Phys. Rev. B **66**, 205403 (2002).

[11] T. L. Chan, C. Z. Wang, M. Hupalo, M. C. Tringides, Z. Y. Lu, and K. M. Ho, Phys. Rev. B **68**, 045410 (2003).

[12] J. N. Crain, K. N. Altmann, C. Bromberger, and F. J. Himpsel, Phys. Rev. B **66**, 205302 (2002).

[13] J. K. Kim, K. S. Kim, J. L. McChesney, E. Rotenberg, H. N. Hwang, C. C. Hwang, and H. W. Yeom, Phys. Rev. B **80**, 075312 (2009).

[14] J. L. McChesney, J. N. Crain, V. Perez-Dieste, F. Zheng, M. C. Gallagher, M. Bissen, C. Gundelach, and F. J. Himpsel, Phys. Rev. B **70**, 195430 (2004).

[15] W. H. Choi, H. Koh, E. Rotenberg, and H. W. Yeom, Phys. Rev. B **75**, 075329 (2007).

[16] W. H. Choi, K. S. Kim, and H. W. Yeom, Phys. Rev. B **78**, 195425 (2008).

[17] K. H. Gundlach, Solid-State Electron. **9**, 949 (1966).

[18] C. L. Lin, S. M. Lu, W. B. Su, H. T. Shih, B. F. Wu, Y. D. Yao, C. S. Chang, and Tien T. Tsong, Phys. Rev. Lett. **99**, 216103 (2007).

[19] J. H. Wu, M. H. Wu, S. Y. Chou, M. C. Yang, S. M. Lu, W. B. Su, and V. Yeh (unpublished).

[20] J. P. Perdew, K. Burke, and M. Ernzerhof, Phys. Rev. Lett. **77**, 3865 (1996).

[21] P. Hohenberg and W. Kohn, Phys. Rev. **136**, B864 (1964); W. Kohn and L. J. Sham, *ibid.* **140**, A1133 (1965).

[22] G. Kresse and D. Joubert, Phys. Rev. B **59**, 1758 (1999).

[23] G. Kresse and J. Hafner, Phys. Rev. B **47**, 558 (1993); G. Kresse and J. Furthmuller, *ibid.* **54**, 11169 (1996).

[24] F. C. Chuang, C. H. Hsu, C. Z. Wang, and K. M. Ho, Phys. Rev. B **77**, 153409 (2008); **78**, 245418 (2008).

[25] T. C. Leung, C. L. Kao, W. S. Su, Y. J. Feng, and C. T. Chan, Phys. Rev. B **68**, 195408 (2003).